The basis of organic spintronics: Fabrication of organic spin valves

2014 Chinese Phys. B 23 018104

(http://iopscience.iop.org/1674-1056/23/1/018104)

TOPICAL REVIEW — Magnetism, magnetic materials, and interdisciplinary research

The basis of organic spintronics: Fabrication of organic spin valves*

Chen Bin-Bin(陈彬彬), Jiang Sheng-Wei(姜生伟), Ding Hai-Feng(丁海峰), Jiang Zheng-Sheng(蒋正生), and Wu Di(吴 镝)†

National Laboratory of Solid State Microstructures and Department of Physics, Nanjing University, Nanjing 210093, *China*

(Received 30 November 2013; published 27 December 2013)

Organic spintronics focuses on utilizing the spin degree of freedom in organic materials because of the long spin relaxation time. The vertical organic spin valve (OSV) is a typical sample structure used to study the spin transport phenomena. However, the fabrication of high quality OSVs is difficult, which results in controversial experiment results and hence hinders the development of organic spintronics. In this work, we describe our recent study on the fabrication of typical vertical organic spin valves, $La_{0.67}Sr_{0.33}MnO_3$ (LSMO)/Alq_3/Co. The LSMO bottom electrodes are annealed to obtain an atomically smooth surface and improved magnetic properties. The top Co electrodes are deposited by an indirect deposition method to reduce the interfusion between Co and Alq_3. The controlled fabrication process provides much better performance and sample yield of OSVs.

Keywords: organic spintronics, organic spin valves, magnetoresistance

PACS: 81.05.Fb, 85.75.–d, 85.70.Kh **DOI:** 10.1088/1674-1056/23/1/018104

1. Introduction

In the past decades, organic semiconductors (SOCs) have attracted considerable interests due to their strong potential applications in electronic devices such as organic light emitting diodes (OLEDs), organic field effect transistors (OFETs), and organic solar cells.[1,2] The displays based on OLEDs are already available in market. In comparison with inorganic semiconductor devices, the organic devices promise several advantages: flexibility, low cost production, fabrication over large surface areas, and almost unlimited materials with tunable properties. On the other hand, spintronics is another rapid developing area which utilizes the spin degree of freedom of electrons to transfer and manipulate information,[3] offering low power and high speed electronic devices.[4] The most successful application of spintronics is the read head in hard disk, leading to an immense increase of the storage density of the hard disk. Recently, the combination of both fields has initiated a new inter-discipline, organic spintronics, to implement the spin functionality in OSCs.

The spin transport mechanism in organic materials is entirely different from that in inorganic systems and very attractive from the fundamental physics point of view due to two distinct characteristics in OSCs. First, the carrier mobility of OSCs is usually very low. Owing to the very weak interaction between the adjacent molecules, the energy bands are narrow, resulting in large effective mass and low mobility. The high-mobility organic films typically have mobility on the order of ~ 1 $cm^2 \cdot V^{-1} \cdot s^{-1}$ for single crystalline films.[5] For most amorphous organic thin films, the electrons tend to be localized with even lower motility. For example, the mobility of the amorphous tris(8-hydroxyquinoline) aluminum (Alq_3) is on the order of $\sim 10^{-5}$ $cm^2 \cdot V^{-1} \cdot s^{-1}$ at room temperature,[6] compared with 450 $cm^2 \cdot V^{-1} \cdot s^{-1}$ for p-type Si. Second, the spin relaxation time in OSCs is much longer than that in inorganic materials. Spin–orbit coupling, hyperfine interaction, and electron–hole interaction are main sources of spin relaxation.[7] Since OSCs are mainly composed of the light atoms, such as C, N, O, and H, the spin–orbit coupling is very weak. As the skeleton of OSCs, C^{12} (98.9% abundance) has no nuclear spin and the carriers mainly transport through C p_z orbitals, suggesting that the hyperfine interaction for the carriers of OSCs is low. In most studies, only one type of carriers, either electrons or holes, carry current, indicating that the electron–hole interaction is absent. Therefore, the spin scattering is extremely weak and consequently the spin relaxation time is very long in OSCs. For example, the spin relaxation time of Alq_3 is about 10^{-3}–1 s,[8] compared with 10^{-12} s for Cu and 10^{-8} s for Si.[9,10]

Stimulated by the development of future spintronic devices and fundamental interests, there have been intense studies on the spin related phenomena in OSCs in the past decade, making this field an active and hot research branch of spintronics.[6,11,12] The very first experiment was carried out in a lateral device geometry $La_{0.67}Sr_{0.33}MnO_3$ (LSMO)/sexithiophene (T_6)/LSMO in 2002.[13] Although magnetoresistance (MR) effects were observed, it was difficult

*Project supported by the National Basic Research Program of China (Grant Nos. 2010CB923402 and 2013CB922103), the National Natural Science Foundation of China (Grant Nos. 11222435, 10974084, and 11023002), the Priority Academic Program Development of Jiangsu Higher Education Institutions, China, and the Fundamental Research Funds for the Central Universities, China.

†Corresponding author. E-mail: dwu@nju.edu.cn

to exclude the MR effects originated from the LSMO Fermi level shift by the external magnetic field.[14] Later, Xiong *et al.* successfully fabricated LSMO/Alq_3/Co vertical organic spin valve (OSV) devices and observed the typical spin-valve loop with 40% MR ratio at low temperature.[11] Motivated by this pioneering work, lots of efforts have been devoted into this field to study the spin related phenomena in OSCs. And several concise reviews of the development in the organic spintronics have been given.[12,15–17]

As already mentioned above, to study the spin transport in OSCs, two types of OSV structures, lateral and vertical structures, are used. The two ferromagnetic (FM) electrodes are in the sample plane with a narrow gap filled with OSCs for lateral OSVs, as shown in Fig. 1(a). Since the carrier mobility of OSCs is very low and the spin diffusion length is about 100 nm or less, the gap is required to be at least comparable to the spin diffusion length to obtain a measurable resistance and MR effects. This makes the fabrication of the lateral OSVs very difficult and thus only a few reports are found to date.[18,19] Considering the high mobility and expected long spin diffusion length for single crystalline OSCs, a few groups tried lateral devices with single crystalline OSCs.[20,21] The sample structure of the vertical OSVs is two FM electrodes separated by an organic spacer to form a sandwich structure, as shown in Fig. 1(b). This sample structure is extensively used due to the simplicity of the sample fabrication. However, the reproducibility and yield of the vertical OSVs are low and controversial results are found, which is an obstacle to hinder the development of organic spintronics. Here we focus on a detail review of our recent progress of fabricating high quality vertical OSVs.

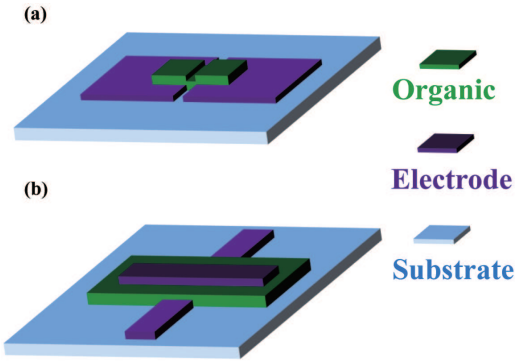

Fig. 1. Schematic representation of typical (a) lateral OSVs and (b) vertical OSVs.

In Section 2, we discuss the deposition and treatment of LSMO films to improve the magnetic properties and the surface morphology. In Section 3, we briefly discuss the deposition of organic thin films. In Section 4, we highlight an indirect deposition method, which is the key improvement of the fabrication of high quality OSVs. Then we compare the results of our OSVs with the previous reported results. In the final section, we summarize the results and briefly outlook the development of organic spintronics.

2. Fabrication of the bottom FM electrode

In the initial lateral and vertical OSVs, LSMO films were used as the electrodes due to their excellent magnetic properties. The spin polarization of LSMO was measured to be nearly 100%,[22] leading to an expected high spin injection efficiency and large MR effects. For example, an MR of more than 1800% was obtained in LSMO-based magnetic tunneling junctions.[23] Since LSMO is an oxide material, it is very stable in ambient air. This allows us to pattern LSMO films by a lithographic process to define proper size and shape without degrading the surface magnetic properties. These two characteristics of LSMO are superior to that of magnetic metals. In fact, the performance of the OSVs using magnetic metals as both electrodes are not as good as that of OSVs using LSMO as the bottom electrodes.[24] In addition, the Curie temperature of LSMO is higher than room temperature. It is possible to obtain room temperature MR effects, which is important for applications. Here, we also choose LSMO films as the bottom FM electrode.

$SrTiO_3$ (001) single crystals are the commonly used substrates to grow LSMO films. To obtain atomically smooth LSMO surfaces, $SrTiO_3$ (100) substrates need to be firstly treated to obtain TiO_2-terminated surfaces.[25] Then the films are epitaxially grown by pulsed laser deposition (PLD) in layer-by-layer growth mode, *in situ* monitored by the intensity oscillation of the reflection high-energy electron diffraction (RHEED) spot. The detailed information about the epitaxial LSMO film growth can be found in our earlier publication.[26] However, the layer-by-layer growth cannot sustain when the film thickness is above ~100 nm, the typical LSMO thickness as the bottom electrode of OSVs, and the process of the growth needs to be carefully controlled.

Here, we provide a simple approach to obtain atomically smooth LSMO films with good magnetic properties. The ~ 100 nm thick LSMO films are grown on $SrTiO_3$ (001) substrates using PLD. The film growth temperature and oxygen pressure are 750 °C and 1×10^{-5} Torr, respectively. The laser energy on the target is 2 J·cm^{-2} with 8 Hz or a higher repetition rate. The ~ 100 nm thick LSMO film is single crystal, as evidenced by the clear RHEED patterns (Fig. 2). The patterned films are obtained by lithographic processes or defined by a shadow mask during growth. The atomic force microscope (AFM) images illustrate relatively smooth surfaces for the as-grown films, as shown in Fig. 3(a), with a root-mean-square roughness of 0.47 nm and peak-to-valley fluctuation of about 1.9 nm. From the temperature dependence of the normalized magnetization curve in Fig. 4, the Curie temperature (T_C) of LSMO films is estimated to be about 320 K, which is well below the T_C of bulk LSMO.

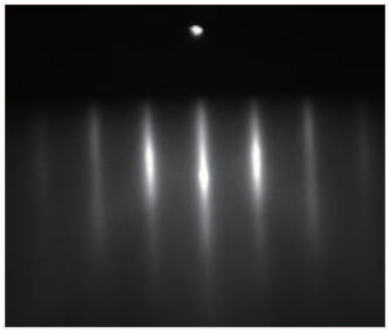

Fig. 2. RHEED pattern of bottom LSMO films.

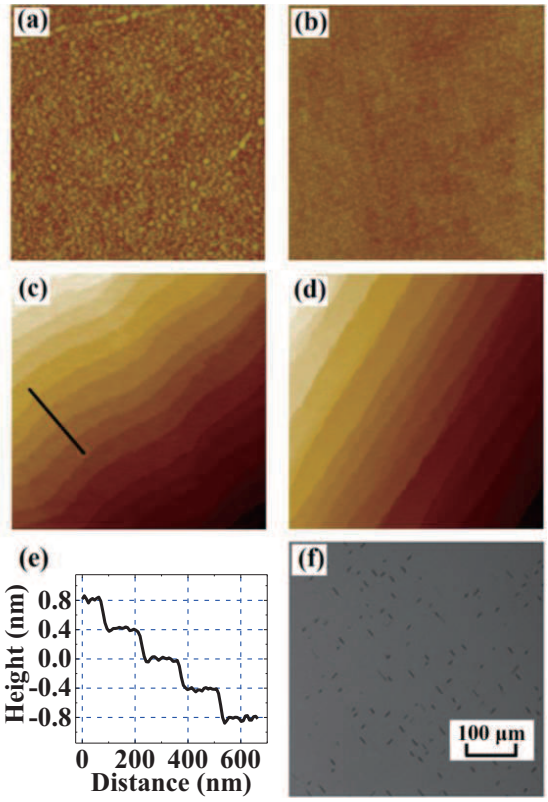

Fig. 3. (a)–(d) AFM images of LSMO films annealed at different temperatures. (e) The line profile of LSMO film as marked by the black line in panel (c). (f) Optical microscope image of the LSMO film annealed at 1200 °C.[30]

The FM interaction in LSMO has been recognized to be the double exchange interaction, in which the local magnetic moment of the Mn ions is mediated by the transfer of the conduction electron through the O ions.[27–29] The oxygen vacancy is generally found in the PLD grown LSMO films. It greatly influences the Mn^{3+}/Mn^{4+} ratio, Mn–O–Mn bond length and bond angle, and therefore the magnetic properties. An annealing process is frequently used to reduce the oxygen vacancy to enhance the magnetization for oxidized materials. Figure 4 displays the temperature dependence of the normalized magnetization for the LSMO films annealed in flowing pure oxygen for 6 h at 1 atm and 900 °C, 1000 °C, 1100 °C, and 1200 °C, respectively. The T_C of all annealed LSMO approaches to the T_C of bulk LSMO, particularly, the film annealed at 1100 °C shows the slowest magnetization decay with increasing temperature.[30] Moreover, the inset of Fig. 4 shows that the saturation magnetization is enhanced after the LSMO film is annealed at 1100 °C.

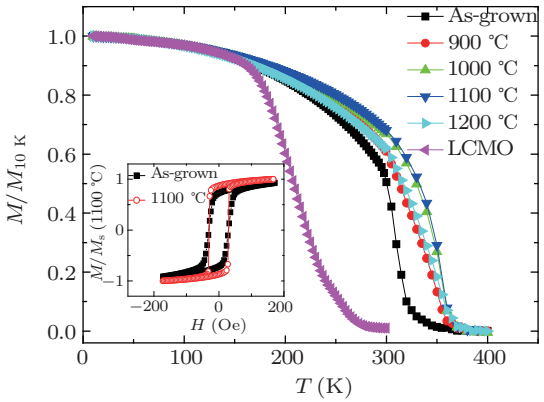

Fig. 4. Temperature dependent normalized magnetization of LSMO films annealed at different temperatures.[30]

The surface morphologies of the annealed LSMO films are partially shown in Fig. 3(b)–3(d), respectively. Obviously, the LSMO film annealed at 1100 °C is the flattest. Several steps with average step height about 0.4 nm in Fig. 3(c) are clearly exhibited in the line profile of Fig. 3(e), marked by a black line. This is corresponding to the lattice constant of LSMO and thus suggests an atomically flat surface. Annealing at high temperature results in step bunching, as shown in Fig. 3(d), and the SrO segregation is clearly observed under optical microscope (Fig. 3(f)). Therefore, we conclude that annealing LSMO at 1100 °C for 6 h is the optimal annealing condition to enhance the FM properties and obtain atomically smooth surfaces.

3. Deposition of the organic thin film

OSC thin films include polymers and small molecules. Several low-cost, low temperature, and solution processing methods are used to prepare the polymer films, such as ink-jet printing, spin-coating, and drop casting. The polymer films are not suitable to be deposited by vacuum evaporation technique due to the decomposition under excessive heat. However, most of the small molecules can be easily evaporated by heating the organic sources to 200–300 °C without decomposition. And the evaporation technique allows one to measure the film thickness by a thickness monitor with a very good precision. In addition, the Langmuir–Blodgett (LB) technique has also been used to prepare the thin films in OSVs. The advantage of this method is that one can control the film thickness at the molecular level.[31,32]

Here, we give an example of preparing small molecule Alq_3 films by thermal deposition. The Alq_3 film thickness is measured by a quartz crystal thickness monitor located next to the sample during the deposition. A thick Alq_3 film

(> 500 nm) is first fabricated to calibrate the thickness monitor by comparing with the surface profiler measurements. Figure 5 shows the surface morphology of 50 nm thick Alq_3, which is deposited on the $SrTiO_3$ (001) substrate at room temperature with a deposition rate of about 0.06 nm/s. The roughness of Alq_3 is as low as 0.4 nm, which is similar with the roughness of Alq_3 films on LSMO. We find that the roughness of organic thin films depends on the substrate temperature, the growth rate, and the organic species.

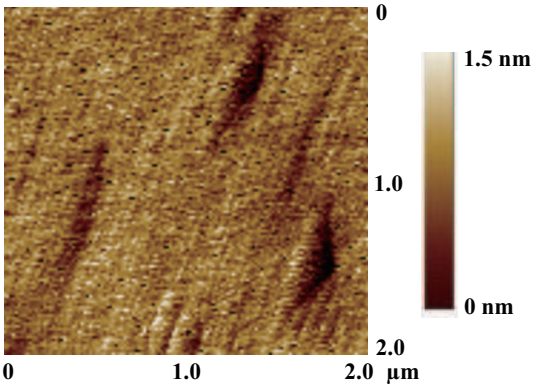

Fig. 5. AFM image of Alq_3 (50 nm) grown on $SrTiO_3$.

4. Deposition of the top FM electrodes

The top FM electrodes are usually directly deposited by thermal deposition, magnetron sputtering, and e-beam deposition, as shown in Fig. 6(a). However, as pointed out by the first report of vertical OSVs, the FM atoms penetrate into the organic layer to form a so-called ill-defined layer due to the high kinetic energy of the vaporized FM atoms. For instance, the ill-defined layer thickness for thermally deposited Co on Alq_3 was measured to be more than 50 nm,[33] which is larger than the spin diffusion length of Alq_3, 45 nm.[11] The ill-defined layer makes the FM/organic interface poor and is the main source causing irreproducible and controversial results.

To reduce the ill-define layer thickness, there are two new approaches reported to deposit the top FM electrodes by other groups. The first one is to deposit a tunnel barrier, such as Al_2O_3 and LiF, on the organic films before depositing the top FM electrodes.[34] The tunnel barriers protect the organic layer during the deposition of the top electrodes. The penetration effects are significantly suppressed and a small room temperature MR effect is observed using this method. This method is very simple and adopted by several other groups.[35] The second approach is called buffer layer assisted growth (BLAG).[36] Before the deposition of the top electrodes, the sample is cooled down to low temperature to condense Xe gas on the organic layer surface to form a buffer layer. The evaporated atoms form clusters on the Xe buffer layer. The clusters have weaker penetration into the organic layer due to the larger size. The Xe buffer layer is desorbed after warming up the samples. A very large MR of more than 300% at low temperature is observed in OSVs of LSMO/Alq_3/Co fabricated by this method.

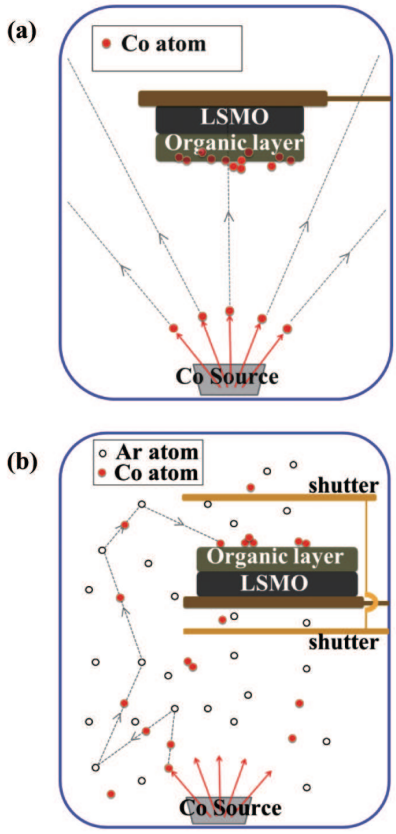

Fig. 6. Schematic diagrams of (a) direct deposition and (b) indirect deposition.[37]

Recently, we developed a new approach called indirect deposition to deposit the top FM electrodes,[37] schematically shown in Fig. 6(b). Unlike the regular direct deposition method, in which the deposition process is accomplished in a high vacuum chamber, the vacuum chamber is intentionally filled with inert Ar gas to lower the vacuum level to about 3×10^{-3} Torr. The vaporized atoms collide with the inert gas to release their kinetic energy. To ensure the vaporized atoms be scattered by the Ar atoms several times, the organic layer covered by a shadow mask is faced away from the electron beam evaporation source, which is from Telemark Inc. with an arc suppression option to operate at low vacuum. We also put a shutter above the sample to let the Co atoms scattered more times. Eventually, the scattered atoms softly land on the organic layer surface and the metal penetration is eliminated. The deposition rate is calibrated to be about 0.004 nm/s, which is $\sim$ 25 times lower than that without Ar gas and with sample facing the evaporation source. Only a fraction of the evaporated metal atoms are deposited on the organic surface, suggesting that most of the metal atoms are deposited on the inner wall of the chamber. The freshly deposited metal films are like a sublimation pump to adsorb non-inert gas, particularly oxygen. Therefore, although the deposition rate is very

low, the deposited metal electrodes are not oxidized if the base pressure is better than 2×10^{-7} Torr. Indeed, we notice that the base vacuum level is better after each indirection deposition. Finally, a thin layer of Al film is directly deposited on Co to prevent from oxidation. We want to point out that the deposition of organic layer and top electrodes is conducted in a chamber without breaking the vacuum to obtain clean interfaces.

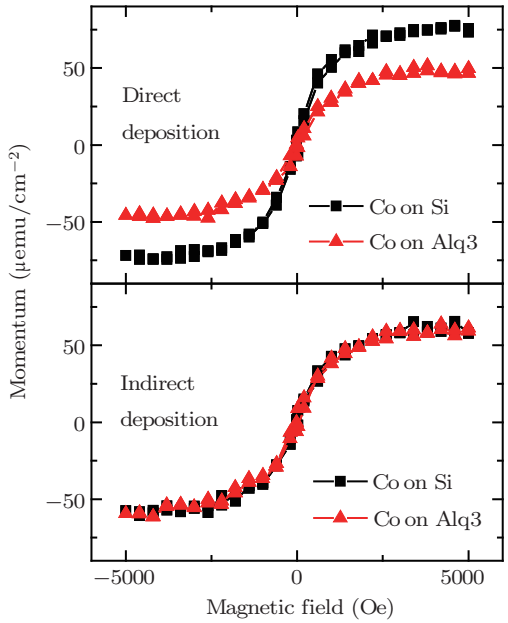

Fig. 7. Room-temperature magnetization hysteresis loops measured by vibrating sample magnetometer (VSM) for Co films on Alq_3 and Si deposited by direct and indirect deposition methods, respectively.[37]

To further confirm the sharp interface obtained at the FM/organic interface by indirect deposition, we compare the magnetic moments of ~ 0.5 nm thick Co films simultaneously deposited on Alq_3 (500 nm)/Si (001) and Si (001) substrates by indirect deposition and direct deposition. To avoid the oxidation of Co, 500 nm thick Alq_3 is deposited as a capping layer after Co deposition. Figure 7 shows the room-temperature hysteresis loops for Co films on Alq_3 and Si deposited by direct and indirect deposition methods, respectively. Clearly, the magnetic moment of Co on Alq_3/Si is smaller than that on Si using the conventional direct deposition. This can be understood by the interfacial intermixing. The intermixing results in enhanced chemical reaction and more Co clusters in the Alq_3 layer, leading to reduced magnetic moments at room temperature. However, for the indirect deposition, the magnetic moment of the Co films on Alq_3/Si is almost the same as that on Si, strongly supporting that the penetration of Co into Alq_3 is significantly suppressed.

5. MR effects of LSMO/Alq_3/Co vertical OSVs

Considering that the most studied OSV structure is LSMO/Alq_3/Co, we fabricated OSVs of this structure and compared our results with the previous reports. Since the LSMO film has an enhanced magnetic moment and a smooth surface morphology after annealing at proper conditions, the impact of the annealed LSMO on the MR effects is studied. For comparison, after the measurements of the OSVs based on the as-grown LSMO (device 1), the same piece of LSMO is annealed at the optimal condition to fabricate OSVs of device 2. Figures 8(a) and 8(b) show the MR loops of devices 1 and 2 with the same device structure LSMO ($\sim$ 100 nm)/Alq_3 (50 nm)/Co (20 nm)/Al (15 nm) measured at 10 K and 2 mV. The MR ratio of device 1 is close to 2%, comparing with that of about 48% for device 2. Importantly, the MR of device 2 persists up to room temperature, as shown in Fig. 8(c), which is not observed in the previous reports in the same device structure.[30] The observed significant improvement of MR is attributed to the improved surface spin polarization after annealing the LSMO films. In fact, we have measured more than 100 LSMO/Alq_3/Co OSVs, the enhancement of the MR ratio was always observed using optimally annealed LSMO as the electrode.

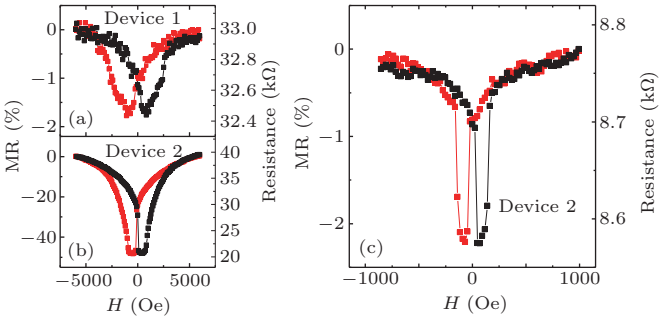

Fig. 8. MR curves of OSV devices fabricated on (a) as-grown LSMO film, (b) optimally annealed LSMO film, respectively, at 10 K. (c) Room temperature MR curve for OSV fabricated on optimally annealed LSMO film.[30]

As previous reported, we found that the LSMO electrodes can be cleaned by a regular process and reused for many times without any apparent degradation, indicating that the surface spin polarization of LSMO is very robust. In addition, the MR behaviors of the *in-situ* fabricated OSVs do not show significant difference from the OSVs based on reused LSMO. Although the LSMO films are inert, they can still react with certain very active organic materials, such as tetrafluorotetracyanoquinodimethane (F4-TCNQ), to lose their magnetic properties. Moreover, we note that the MR ratio and the resistance of the same sample structure varies from sample to sample. However, the variation is significant smaller for the samples fabricated on the same piece of LSMO. This is probably due to the sensitivity of the work function and spin polarization of LSMO to the oxygen content, which is difficult to control in experiments.[38]

To further confirm that the indirect deposition method can reduce the inter-diffusion at the FM/organic interfaces, we fabricated OSVs with a relative thin Alq_3 layer. Figure 9(a) shows

a typical MR loop of an LSMO (100 nm)/Alq_3 (25 nm)/Co (20 nm)/Al (15 nm) OSV at 15 K and $V = 0.1$ V, in which the organic layer thickness is much thinner than that in the previous reports and is beyond the tunneling regime but in the range of ill-define thickness. The resistance of two FM electrodes in the parallel configuration is higher than that in the antiparallel configuration, i.e., negative MR. The negative MR is observed in the entire bias voltage range and the MR ratio monotonically decreases with increasing bias voltage regardless of the polarity of the voltage as shown in Fig. 9(b), consistent with the previous reports in which a much thicker Alq_3 was used and the Co electrode was directly deposited.[11] In OSVs fabricated by the regular direct deposition methods, 25 nm thick Alq_3 films would lead to short circuits. Clearly, the indirect deposition method significantly reduces the Co penetration into the organic layer to obtain high quality samples.

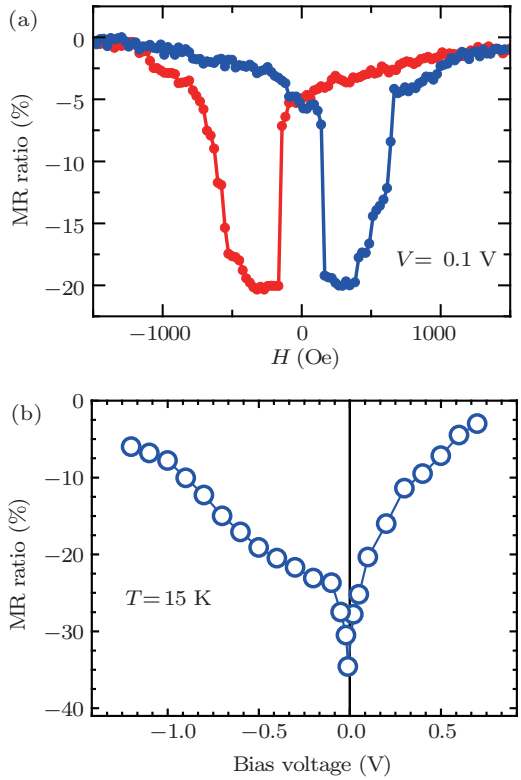

Fig. 9. (a) MR curve for OSV device of LSMO (100 nm) / Alq_3(25 nm) / Co(20 nm) / Al(15 nm) measured at 15 K with a bias voltage of 0.1 V. (b) The MR as a function of the bias voltage measured at 15 K.

6. Summary and outlook

We systematically studied every step of fabricating vertical OSVs. Here, we emphasize that the annealed LSMO bottom electrode and the indirect deposited top electrode are crucial for high quality OSVs. The annealing LSMO films in flowing oxygen at 1100 °C make the surface morphology atomically flat and improve the magnetic property close to the bulk materials. The indirect deposition method reduces the penetration of metal atoms into the organic layer during deposition to obtain a sharp FM/organic interface. The improved LSMO films and Alq_3/Co interfaces have led to the significant increase of the MR effects and the room temperature MR effects. Moreover, the reproducibility of OSVs is greatly improved.

Organic spintronics is a rapidly developing branch of spintronics due to its rich physics and exciting possible applications. In the fundamental physics aspect, the spin injection and the relaxation mechanisms are still not well understood and under hot debate. It is well accepted that the role of the FM/organic interface is important in spin injection.[35,39,40] Engineering the FM/organic interface is the key to study the physical mechanisms. Although a lot of works have been done, the impact of the interface on the spin injection in OSVs is not well understood. The spin relaxation mechanisms based on spin–orbit coupling and hyperfine interaction are both supported by experiments and theories.[8,41–43] In addition, the Hanle effect,[44] which is caused by the precession of the spin in the presence of a non collinear magnetic field in the non-magnetic spacer during transport, already observed in metallic and inorganic semiconductors, is still absent in organic materials.[45] Its observation is believed to be a conclusive experiment to demonstrate the transport of the injected spin. In the application aspect, the OLEDs are recently demonstrated to control the light emission intensity by manipulating the spin,[44] and an electrically controlled OSV which combines the GMR effect and the electrical memory effect is realized.[47] Recently, utilizing the hybridization and magnetic exchange interaction between organic molecules and the surface of the FM, an interface magnetoresistance effect[48] is observed, showing the application potential for building molecular-scale quantum spin memory and processors for technological development. Moreover, the spin transport at the molecule scale is intensively studied, which is important to understand and manipulate the spin transport in organic thin films.[49–51] Organic spintronics is still in its infancy and many open questions are still there waiting for us to answer.

References

[1] Rorrest S R 2004 *Nature* **428** 911
[2] Braga D and Horowitz G 2009 *Adv. Mater.* **21** 1473
[3] Wolf S A, Awschalom D D, Buhrman R A, Daughton J M, von Molnar S, Roukes M L, Chtchelkanova A Y and Treger D M 2001 *Science* **294** 1488
[4] Bratkovsky A M 2008 *Rep. Prog. Phys.* **71** 026502
[5] Park S K, Jackson T N, Anthony J E and Mourey D A 2007 *Appl. Phys. Lett.* **91** 063514
[6] Szulczewski G, Sanvito S and Coey M 2009 *Nat. Mater.* **8** 693
[7] Zutic I, Fabian J and Sarma S D 2004 *Rev. Mod. Phys.* **76** 323
[8] Pramanik S, Stefanita C G, Patibandla S, Bandyopadhyay S, Garre K, Harth N and Cahay M 2007 *Nat. Nanotech.* **2** 216
[9] Bass J and Pratt W P 2007 *J. Phys.: Condens. Matter* **19** 183201
[10] Appelbaum I, Huang B and Monsma D 2007 *Nature* **447** 295
[11] Xiong Z H, Wu D, Vardeney Z V and Shi J 2004 *Nature* **427** 821
[12] Dediu V, Hueso L, Bergenti I and Taliani C 2009 *Nat. Mater.* **8** 707

[13] Dediu V, Murgia M, Matacotta F C, Taliani C and Barbanera S 2002 *Solid State Commun.* **122** 181

[14] Wu D, Xiong Z H, Li X G, Vardeny Z V and Shi J 2005 *Phys. Rev. Lett.* **95** 016802

[15] Naber, W J M, Faez S and van der Wiel W G 2007 *J. Phys. D* **40** R205

[16] Sanvito S 2011 *Chem. Soc. Rev.* **40** 3336

[17] Jiang S W, Yue F J, Wang S and Wu D 2013 *Sci. China-Phys. Mech. Astron.* **56** 142

[18] Ikegami T, Kawayama I, Tonouchi M, Nakao S, Yamashita Y and Tada H 2008 *Appl. Phys. Lett.* **92** 153304

[19] Ozbay A, Nowak E R, Yu Z G, Chu W, Shi Y, Krishnamurthy S, Tang Z and Newman N 2009 *Appl. Phys. Lett.* **95** 232507

[20] Naber W J M, Craciun M F, Lemmens J H J, Arkenbout A H, Palstra T T M, Morpurgo A F and van der Wiel W G 2010 *Org. Electron.* **11** 743

[21] Burke F, Stamenov P and Coey J M D 2011 *Synth. Met.* **161** 563

[22] Park J H, Vescovo E, Kim H J, Kwon C, Ramesh R and Venkatesan T 1998 *Phys. Rev. Lett.* **81** 1953

[23] Bowen M, Bibes M, Barthelemy A, Contour J P, Anane A, Lemaitre Y and Fert A 2003 *Appl. Phys. Lett.* **82** 233

[24] Wang F J, Xiong Z H, Wu D, Shi J and Vardeny Z V 2005 *Syth. Metals* **155** 172

[25] Koster G, Kropman B L, Rijnders G J H M, Blank D H and Rogalla H 1998 *Appl. Phys. Lett.* **73** 2920

[26] Shi Y J, Zhou Y, Ding H F, Zhang F M, Pi L, Zhang Y H and Wu D 2012 *Appl. Phys. Lett.* **101** 122409

[27] Zener C 1951 *Phys. Rev.* **82** 403

[28] Millis A J, Littlewood P B and Shraiman B I 1995 *Phys. Rev. Lett.* **74** 5144

[29] Millis A J 1996 *Phys. Rev. B* **53** 8434

[30] Chen B B, Zhou Y, Wang S, Shi Y J, Ding H F and Wu D 2013 *Appl. Phys. Lett.* **103** 072402

[31] Yu T, Zhang Q T, Liu D P and Han X F 2013 *Appl. Phys. Lett.* **102** 022401

[32] Tai J C, Huang J C, Chang Y M, Li K S, Hong J Y, Wong S S, Chiang W C and Lin M T 2010 *Appl. Phys. Lett.* **96** 262502

[33] Vinzelberg H, Schumann J, Elefant D, Gangineni R B, Thomas J and Bühner B 2008 *J. Appl.Phys.* **103** 093720

[34] Dediu V, Hueso L E, Bergenti I, Riminucci A, Borgatti F, Graziosi P, Newby C, Casoli F, De Jong M P, Taliani C and Zhan Y 2008 *Phys. Rev. B* **78** 115203

[35] Schulz L, Nuccio L, Willis M, Desai P, Shakya P, Kreouzis T, Malik V K, Bernhard C, Pratt F L, Morley N A, Suter A, Nieuwenhuys G J, Prokscha T, Morenzoni E, Gillin W P and Drew A J 2011 *Nat. Mater.* **10** 39

[36] Sun D, Yin L, Sun C, Guo H, Gai Z, Zhang X G, Ward T Z, Cheng Z and Shen J 2010 *Phys. Rev. Lett.* **104** 236602

[37] Wang S, Shi Y J, Lin L, Chen B B, Yue F J, Du J, Ding H F, Zhang F M and Wu D 2011 *Syth. Metals* **161** 1738

[38] Li F, Zhan Y, Lee T H, Liu X, Chikamatsu A, Guo T F, Lin H J, Huang J C A and Fahlman M 2011 *J. Phys. Chem. C* **115** 16947

[39] Yue F J, Shi Y J, Chen B B, Ding H F, Zhang F M and Wu D 2012 *Appl. Phys. Lett.* **101** 022416

[40] Steil S, Groβmann N, Laux M, Ruffing A, Steil D, Wiesenmayer M, Mathias S, Monti O L A, Cinchetti M and Aeschlimann M 2013 *Nat. Phys.* **9** 242

[41] Drew A J, Hoppler J, Schulz L, Pratt F L, Desai P, Shakya P, Kreouzis T, Gillin W P, Suter A, Morley N A, Malik V K, Dubroka A, Kim K W, Bouyanfif H, Bourqui F, Bernhard C, Scheuermann R, Nieuwenhuys G J, Prokscha T and Morenzoni E 2008 *Nat. Mater.* **8** 109

[42] Yu Z G 2011 *Phys. Rev. Lett.* **106** 106602

[43] Nguyen T D, Hukic-Markosian G, Wang F, Wojcik L, Li X G, Ehrenfreund E and Vardeny Z V 2010 *Nat. Mater.* **9** 345

[44] Johnson M and Silsbee R H 1985 *Phys. Rev. Lett.* **55** 1790

[45] Riminucci A, Prezioso M, Pernechele C, Graziosi P, Bergenti I, Cecchini R, Calbucci1 M, Solzi M and Alek Dediu V 2013 *Appl. Phys. Lett.* **102** 092407

[46] Nguyen T D, Ehrenfreund E and Vardeny Z V 2012 *Science* **337** 204

[47] Prezioso M, Riminucci A, Bergenti I, Graziosi P, Brunel D and Dediu V A 2011 *Adv. Mater.* **23** 1371

[48] Raman K V, Kamerbeek A M, Mukherjee A, Atodiresei N, Sen T K, Lazić P, Caciuc V, Michel R, Stalke D, Mandal S K, Blügel S, Münzenberg M and Moodera J S 2013 *Nature* **493** 509

[49] Rocha A R, García-suárez V M, Bailey S W, Lambert C J, Ferrer J and Sanvito S 2005 *Nature Mater.* **4** 335

[50] Wang S, Yue F J, Shi J, Shi Y J, Hu A, Du Y W and D Wu 2011 *Appl. Phys. Lett.* **98** 172501

[51] Sanvito S 2011 *Chem. Soc. Rev.* **40** 3336